Nanostructured Polyaniline/Titanium Dioxide Composite Anode for Microbial Fuel Cells

Yan Qiao,[†,‡] Shu-Juan Bao,[†,‡] Chang Ming Li,[†,‡,*] Xiao-Qiang Cui,[†,‡] Zhi-Song Lu,[†,‡] and Jun Guo[§]

[†]School of Chemical and Biomedical Engineering, [‡]Center for Advanced Bionanosystems, and [§]School of Materials Science and Engineering, Nanyang Technological University, 70 Nanyang Drive, Singapore 637457

ABSTRACT A unique nanostructured polyaniline (PANI)/mesoporous TiO_2 composite was synthesized and explored as an anode in *Escherichia coli* microbial fuel cells (MFCs). The results of X-ray diffraction, morphology, and nitrogen adsorption–desorption studies demonstrate a networked nanostructure with uniform nanopore distribution and high specific surface area of the composite. The composite MFC anode was fabricated and its catalytic behavior investigated. Optimization of the anode shows that the composite with 30 wt % PANI gives the best bio- and electrocatalytic performance. A possible mechanism to explain the excellent performance is proposed. In comparison to previously reported work with *E. coli* MFCs, the composite anode delivers 2-fold higher power density (1495 mW/m^2). Thus, it has great potential to be used as the anode for a high-power MFC and may also provide a new universal approach for improving different types of MFCs.

KEYWORDS: polyaniline · mesoporous titanium dioxide · *Escherichia coli* · microbial fuel cells · electrocatalysis

Microbial fuel cells (MFCs) as one type of "green" energy source have attracted great interest among researchers. In MFCs, the use of entire microorganisms as microreactors eliminates the need for isolation of individual enzymes and allows active biomaterials under conditions close to their natural environment to convert organic compounds, from simple carbohydrates to waste organic matter, into electricity at a high efficiency. Thus, the use of MFCs has great potential for broad applications, particularly in home electrical generators, electronic power sources for space shuttles, and self-feeding robots.[1] However, the low power density and poor long-term stability limit its practical applications.[2,3] Although a number of factors can affect a MFC's performance,[3–5] the anode electrode associated with microbial inoculums has the greatest impact on its power density. In the past few years, some scientists have improved the MFC anode material by impregnating it with different chemical catalysts.[6–8] Optimization of the porous structure of the electrode with higher specific surface area increases the apparent power density, but it is observed that the pores are clogged by the entering bacteria, resulting in cell death and significant reduction of the electrochemical reaction surface.[9] Conventional carbon-based anodes, such as carbon felts and porous carbon papers, suffer too from this very challenging problem.[9]

Polyaniline (PANI) is a popular conducting polymer due to its simple synthesis process, good electrical conductivity, and environmental stability,[10] and it has been studied for use as a MFC anode through modifications. Recently, Schröder *et al.* employed PANI to modify a platinum anode for MFC[11] and achieved a current density 1 order of magnitude higher than the previously reported value. PANI/inorganic composites are also reported to have better conductivity.[12,13] Our previous work[14] has demonstrated that a favorable nanostructure of a carbon nanotube/PANI composite anode improves the MFC performance, especially the power density.

It is a great challenge to develop a new anode material to further increase the power density of a MFC. The nature of the catalytic mechanism of a MFC anode involves not only a bio- but also an electrocatalytic process. An optimal nanostructure with high specific surface area favorable for both catalytic processes could play a critical role in improving the MFC power density; such a structure needs to host the bacteria with high bioactivity while enhancing the electron-transfer rate. Mesoporous structured inorganic materials have a large specific surface area and uniform pore distribution. Among these materials, TiO_2 is biocompatible, stable, and environmentally friendly,[15] and its electronic, optical, and dielectric properties can be enhanced by surface modifications[16–19] to allow it to be

*Address correspondence to ecmli@ntu.edu.sg.

Received for review July 16, 2007 and accepted November 29, 2007.

Published online December 14, 2007.
10.1021/nn700102s CCC: $40.75

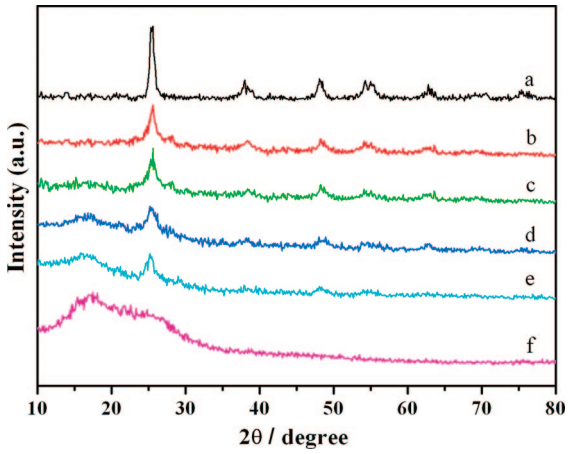

Figure 1. X-ray diffraction of (a) TiO_2, (b) 10 wt % PANI/TiO_2, (c) 20 wt % PANI/TiO_2, (d) 30 wt % PANI/TiO_2, (e) 50 wt % PANI/TiO_2, and (f) PANI.

used for a MFC anode. However, TiO_2 has low electric conductivity that limits its use for high power output.

We have recently synthesized a new mesoporous TiO_2 electrode material with uniform nanopore distribution and high specific surface area.[20] In this work, we use this material to fabricate a unique nanostructured PANI/TiO_2 composite for the MFC anode. Both biocatalytic and electrocatalytic properties of the composite are optimized by tailoring the composition ratio. The optimal composite is employed in an *Escherichia coli* MFC, and the power density is examined. To the best of our knowledge, this new hybrid polymer/inorganic porous composite is for the first time fabricated and applied to MFCs.

RESULTS AND DISCUSSION

Characterization of PANI/TiO_2 Composites. The phases of both TiO_2 and the PANI/TiO_2 composite were determined by X-ray diffraction (XRD, Figure 1). Curve a displays the characteristic patterns of TiO_2, and the main peaks can be indexed to the anatase TiO_2 phase (JCPDS, card no. 21-1272). Curve f shows that the plain PANI has a certain degree of crystallinity. The broad peak can be ascribed to the scattering from polyaniline chains at interplanar spacing. The patterns of the four composites indicate that PANI deposited on the surface of TiO_2 has no effect on the crystallization characteristics of TiO_2. With increasing PANI percentage in the composite, the intensity of the broad peak of PANI is enhanced. This may suggest that the crystalline behavior of PANI is not hampered by the restrictive effect of the surface of TiO_2 as reported in the literature.[16] However, the intensity of the characteristic peaks of TiO_2 is dampened by the increase in the thickness of the polymer layer.

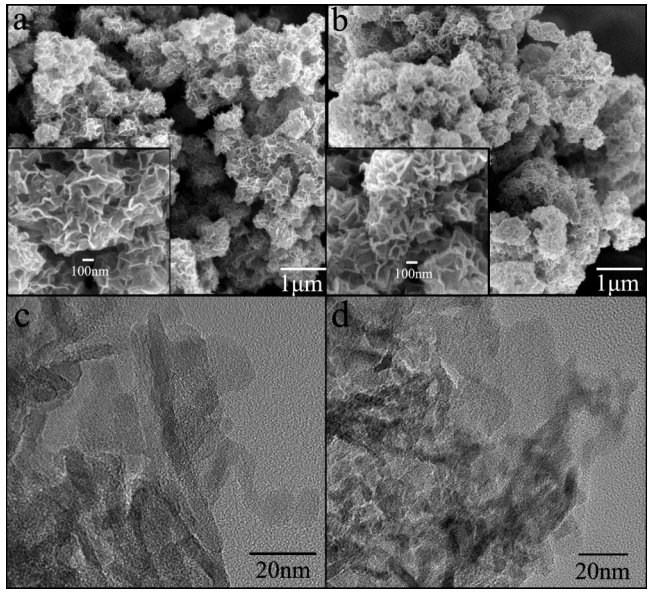

Figure 2. SEM (a,b) and TEM (c,d) micrographs of TiO_2 (a,c) and PANI/TiO_2 composite (b,d) with 30 wt % PANI. The insets are the high-magnification graphs.

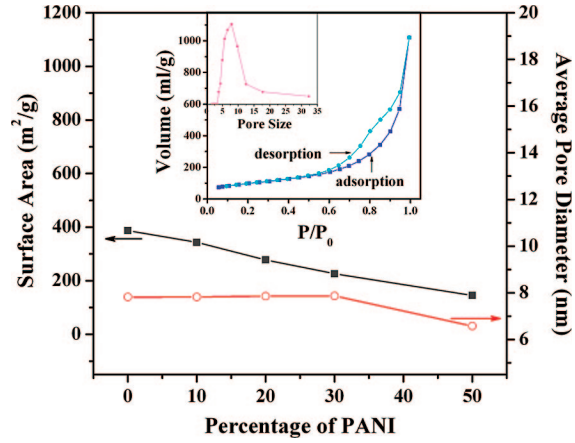

Figure 3. Specific surface area and average pore diameter of PANI/TiO_2 nanocomposites. The insets are the N_2 adsorption–desorption isotherm (big) and BJH pore size distribution (small) of the composites containing 30 wt % PANI.

The morphologies (Figure 2) of both TiO_2 and the PANI/TiO_2 composite were examined by field emission scanning electron microscopy (FESEM) and transmission electron microscopy (TEM). Figure 2a demonstrates that TiO_2 agglomerates to form a loose nanostructure with uniform nanopore distribution. The SEM micrograph with high magnification (inset of Figure 2a) clearly shows that the TiO_2 cluster consists of flakes that cross-link with each other to form a porous network. The composite structure (Figure 2b) is more compact than TiO_2, and the graph with high magnification (inset of Figure 2b) reveals that the porous flake-cross-linked structure of the mesoporous TiO_2 is retained after PANI modification. The TEM micrographs (Figure 2c,d) also illustrate the nanoflake structure for the composite, not significantly different from that of TiO_2.

The results of specific surface area and average pore diameter are shown in Figure 3; the inset shows the N_2 adsorption–desorption isotherm and the pore distribution of the PANI/TiO_2 nanocomposite with 30 wt % PANI. The composite (Figure 3) has a high specific surface area above 150 m^2/g, which is larger by 300 times

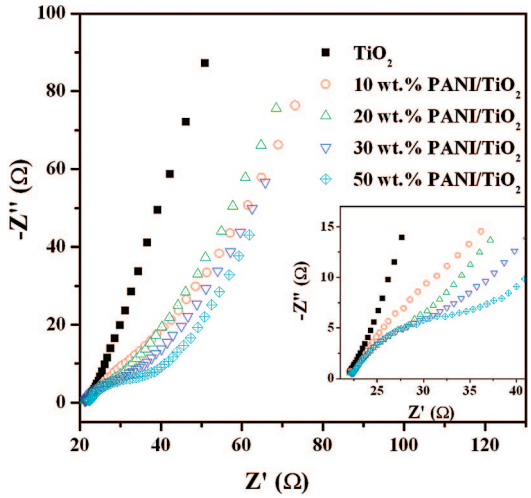

Figure 4. Nyquist plots on different electrodes in an anaerobic culture of *E. coli* K-12 containing 55 mM glucose, 0.5 mM HNQ, and 0.1 M phosphate buffer (pH 7.0).

than that of woven graphite felt (about 0.5 m^2/g),[6,21] a widely used anode material in MFCs. The specific surface area decreases with increasing PANI content in the composite. This could possibly be attributed to the lower specific surface area of PANI than TiO_2, deposition of which could reduce the specific surface area of the composite. The isotherm has a hysteretic loop, which is a characteristic of the adsorption–desorption of a porous material. The inset of Figure 3 also shows a narrow and uniform pore size distribution of the composite, with an average pore diameter over in the range of 6–8 nm, which is much smaller than the diameter of the bacteria (about 0.5–2 μm). Thus, the bacteria cannot enter into and clog the pores, causing their death from lack of nutrients[9] and reduction of the reaction surface area as well. The results obtained for TiO_2 and other composites with different percentages of PANI are similar to those shown in Figure 3 and are not presented here.

Catalytic Behavior of PANI/TiO_2 Composite Electrodes. The complex impedance (*Z*) *vs* frequency, known as a Nyquist plot, was measured with TiO_2 and four composite electrodes in an anaerobic culture of *E. coli* K-12 with 55 mM glucose and 5 mM 2-hydroxy-1,4-naphthoquinone (HNQ) (Figure 4); the inset in Figure 4 illustrates the high-frequency part of the result. The Nyquist plots of all four composite electrodes represent well-defined frequency-dependent semicircle impedance curves over high frequencies followed by straight lines, but the TiO_2 electrode has no defined semicircle. A Randle equivalent circuit[21] is often used to model the complex impedance in an electrochemical cell, in which the charge-transfer resistance (R_{ct}) at the electrode/electrolyte interface is equal to the diameter of the semicircle. Smaller R_{ct} indicates a faster electron-transfer rate. The result in Figure 4 indicates that R_{ct} is remarkably reduced after PANI deposits on TiO_2 and is further decreased with increasing PANI content in the composite electrode. However, after 20 wt % PANI is deposited on TiO_2, further increasing the PANI content has no significant effect on reducing R_{ct}. The results here reveal that TiO_2 has no electrocatalysis on glucose oxidation, and its catalytic performance can be significantly improved by PANI deposition on its surface. This can possibly be ascribed to the fact that addition of PANI forms a nanostructured network (Figure 2), which could enhance the electron-transfer rate. At low frequencies, the inclined line with a slope higher than 45° and close to 90° demonstrates a capacitive-like behavior, characteristic of a porous conducting film.[22–24]

The cyclic voltammograms (CVs) shown in Figure 5A were measured in 0.1 M phosphate buffer> + *E. coli* cells + 5 mM HNQ, and they all have a pair of well-defined redox waves, obviously due to redox reaction of HNQ. The charge capacities calculated from the CVs (inset of Figure 5A) show that the charge capacity increases with increasing PANI content in the composites up to 30 wt %, at which the maximum value is reached and then decreases with further increase of PANI content. Because the charge capacity of an electrode for a specific reaction is known to be proportional to the electrode surface, this result indicates that the reaction surface area increases with increasing PANI content until reaching its maximum and then decreases with further increase of PANI content. The CVs in Figure 5B were measured in 0.1 M phosphate buffer + *E. coli* cells + 5 mM HNQ + 55 mM glucose, and the cur-

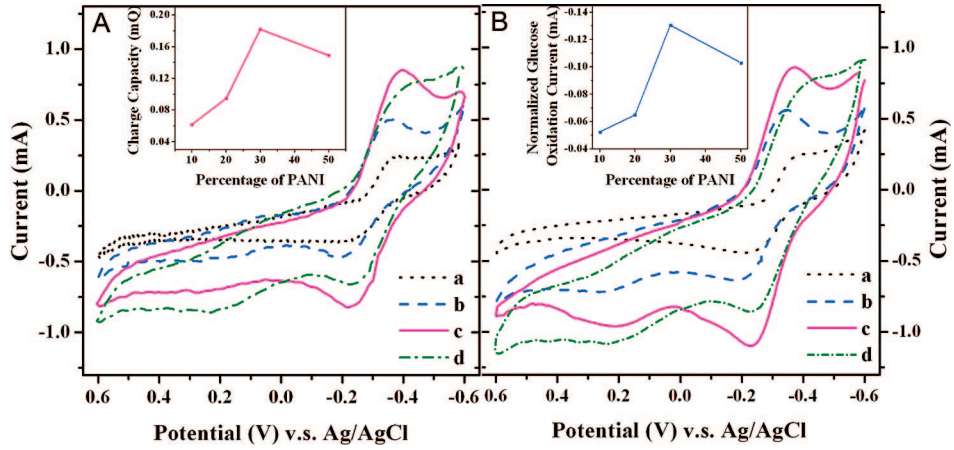

Figure 5. Cyclic voltammograms of different PANI/TiO_2 composite electrodes in an anaerobic suspension of *E. coli* K-12 containing 5 mM HNQ without glucose (A) and with 55 mM glucose (B): (a) 10 wt % PANI/TiO_2; (b) 20 wt % PANI/TiO_2; (c) 30 wt % PANI/TiO_2; and (d) 50 wt % PANI/TiO_2. Scan rate, 5 mV/s. The inset of panel A displays the charge capacity of the different electrodes. The inset of panel B represents the baseline-subtracted peak current of glucose oxidation.

rent axis has the same scale as that in Figure 5A for comparison. Similarly to panel A, panel B also exhibits a pair of well-defined redox waves. However, panel B has significant differences in comparison to panel A; for instance, the anodic peak current is much larger than its cathodic one. In addition, for the electrodes with same percentage of PANI, the anodic peak current in panel B is much larger than that in panel A, although their cathodic peak currents are almost identical. Apparently, the larger anodic current is due to the glucose oxidation. After subtracting the background produced by HNQ, only the anodic waves can be observed (not shown in Figure 5), revealing that the glucose oxidation on the *E. coli*−PANI/TiO_2 electrode is a totally irreversible electrochemical reaction. This is in agreement with our reported works.[25,26] The redox potential range of the glucose oxidation, from −0.4 to −0.2 V (Figure 5B), is as same as that of HNQ (Figure 5A), indicating that HNQ is an electron-transfer mediator between the nonconductive *E. coli* cells and the electrode.[27,28] The inset in Figure 5B clearly shows that the relationship of anodic peak current of the glucose oxidation *vs* PANI percentage in the composites has the same trend as the relation of charge capacity *vs* PANI percentage (inset in Figure 5A). The highest peak current, for glucose oxidation with 30% PANI composite electrode, indicates the best bio- and electrocatalysis of the glucose oxidation.

The peak current of a totally irreversible electrochemical reaction in CV is proportional to the electrode surface (A), bulk reactant concentration (C_0), and reactant diffusion coefficient (D_0).[21] In Figure 5, C_0 and D_0 can be considered roughly constant. As discussed above, the effective reaction surface of the electrode is proportional to its charge capacity. That is why the relationship of the peak current of glucose oxidation *vs* PANI percentage in the composites has the same change trend as that of the charge capacity *vs* the PANI percentage (insets in Figure 5A,B). However, both charge capacity (Figure 5A) and peak current (Figure 5B) do not simply increase with increasing PANI content in the composite. It is known that a porous electrode has a high internal surface area and, therefore, gives high electrochemical rates per apparent unit surface area of electrode, but the internal area cannot, in general, be completely utilized at high current densities due to the internal effect from mass transfer and ohmic polarization in an electrolyte that is simply dependent on the pore structure.[29] On the basis of the porous electrode theory, it is possible to explain why there is an optimal PANI percentage in the composite for the best bio- and electrocatalytic behavior. Figure 3 illustrates that the average pore size of the electrodes remains constant with increasing PANI content in the composite up to 30% but then decreases with further PANI increases. This may suggest that the pore structure and the utility of the electrodes are mainly determined by the TiO_2 microstructure after the PANI deposits up to 30 wt % of the composite. In fact, FESEM and TEM results (Figure 2) show that the fundamental nanoflake pore structure of TiO_2 is not changed significantly after modification with PANI, and thus the electrode surface area can increase with increasing PANI deposit. However, when the PANI content is more than 30%, the average pore size decreases, and the internal effect could become the controlling factor in decreasing the electrode utility caused by reduced mass transport and higher IR polarization in the electrolyte, which suppresses the electrocatalytic current.

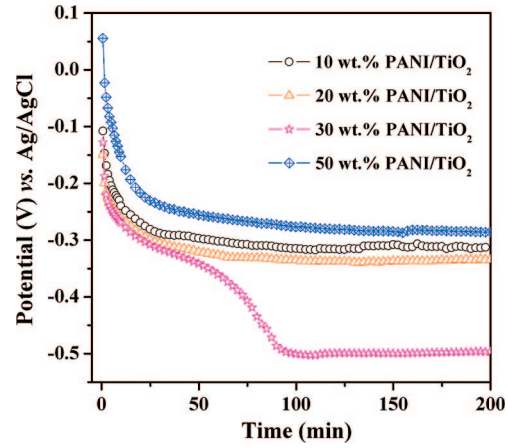

Figure 6. Potential−time curve of anode-limiting MFCs utilizing different PANI/TiO_2 composites as anodes.

In order to explore the discharge profile of different composite anodes, an anode-limiting MFC was designed, in which the Pt cathode had much larger surface area than that of the anode and thus the cathode polarization is insignificant. The volume of the MFC was 25 mL, and the concentration of *E. coli* cells was about 1×10^9 cells mL^{-1}, while the concentrations of HNQ and glucose were as same as those in the experiments described above. The constant current discharge experiments using the MFC with the four different anodes were conducted at 0.1 mA/cm^2, resulting in a change of the anode potential (*vs* Ag/AgCl) *vs* the discharge time as shown in Figure 6. For an anodic reaction, the more negative the anode discharge potential, the better the electrocatalysis. Apparently, the composite anode with 30 wt % PANI gives much more negative potential (−0.5 V *vs* Ag/AgCl) during the discharge, demonstrating that it has the best electrocatalytic performance among the tested composites, which is in agreement with the CV results shown in Figure 5. As we discussed above, the greatest electrocatalytic behavior of the *E. coli*−30 wt % PANI/TiO_2 electrode could be ascribed to optimal pore structure for good mass transfer and low IR drops in the inner pores. Figure 6 also illustrates that the discharge profile of the composite/bacteria anode is totally different from that of a conventional anode: the bacteria anode has a high polarization potential initially that gradually becomes lower with increasing discharge time and finally becomes

constant at its lowest polarization potential. This is possibly due to the bacteria growth process. In our experiments, the discharge process started immediately after addition of glucose solution and bacteria, which need time to grow to their maximum metabolic level and to distribute into the inner surface of the anode for the best performance. In addition, Figure 6 also shows a prominent feature of the 30 wt % PANI/TiO_2 composite: its catalytic effect, after reaching its maximum, is much more significantly improved than that of the other composite electrodes relative to their initial electroactivity, possibly indicating that it offers the best nanostructure environment for bacteria growth, which will be discussed more in the next section.

Bacteria Behaviors on PANI/TiO_2 Composite Surface. After discharge, the surface morphology of the PANI/TiO_2 composite anode was immediately examined with FESEM (Figure 7). It is seen that the *E. coli* cells on the electrode surface produce some hairlike structures, which are reported as pili to allow bacteria to attach to other cells and to play a key role in mediation of the bacteria movement and biofilm formation.[30,31] Obviously, the pili could also promote cell adhesion on the composite surface, the host substrate. Figure 7a shows that lots of *E. coli* cells accumulate on the electrode surface and adhere to one another by pili. The graphs with high magnification (Figure 7b,c) clearly illustrate that the extended pili attach the cells on the electrode surface and cross-link each other to form a network. This phenomenon is not found on free-floating cells in the electrolyte (Figure 7d). One possible reason is that the rough surface of the electrode could stimulate the cell to produce the pili and then to firmly attach the cells onto the electrode surface for a superior biofilm by pili cross-linking,[32] in which the bacteria can have a sound environment for extracellular electron transfer during the electrochemical reaction.[33,34] It is reported that the pili of some metal-reducing bacteria are highly conductive and thus can directly transfer electrons to electrodes like a cable.[35,36] Possibly, the pili of *E. coli* cells on the composite electrode surface could also facilitate electron transfer between the cells and electrode, which could even play a key role in mediatorless *E. coli* MFCs[37,38] and currently is under investigation in the author's laboratory. Figure 7c shows a superior *E. coli* pili network, indicating that the nanostructured PANI/TiO_2 composite electrode is an excellent host for cell growth.

Performance of the PANI/TiO_2 Anode in a MFC. The performance of the PANI/TiO_2 anode was tested in a dual-chamber MFC system that was constructed from two glass bottles (450 mL capacity) joined by a glass tube installed with a 1.5-cm-diameter proton exchange membrane (PEM, Nafion 117, Dupont, Wilmington, DE). The anode (1.5 cm × 1.5 cm) was made of 30 wt % PANI/TiO_2 composite (the best performer as discussed above), the compartment of which contained an anaerobic growing suspension of *E. coli* K-12 cells inoculated

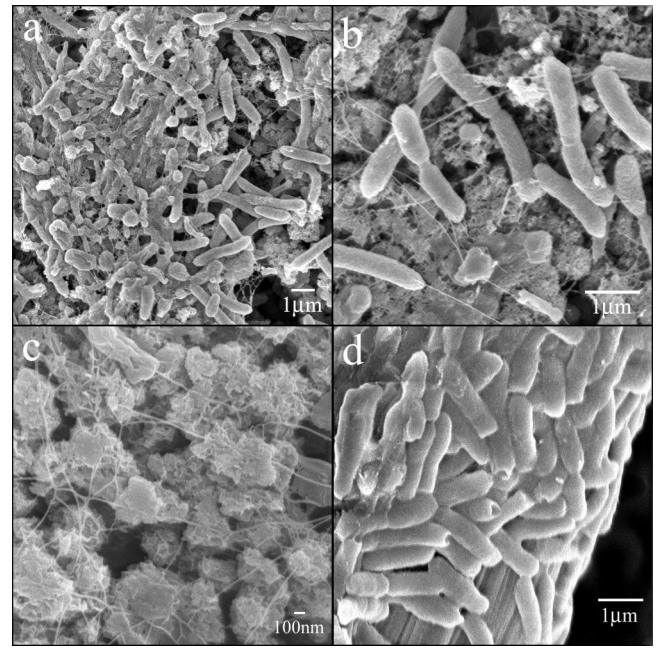

Figure 7. SEM micrographs of *E. coli* cells adhered on a 30 wt % PANI/TiO_2 electrode surface (a−c) and free-floating cells (d).

in a medium just before the test. The cathode was as-received carbon cloth (E-TEK, B1D), and the catholyte was a 50 mM ferricyanide solution with phosphate buffer identical to that in the bacterial medium. Current and potential measurements on the MFC were carried out by using a benchtop digital multimeter (ESCORT 3146A) during discharge in constant-load mode with an external resistance of 1.95 kΩ, and the result is shown in Figure 8. It is noted that, after bacteria enrichment for about 48 h, the power density rises to a plateau and remains there for about 450 h without addition of glucose or other nutrition. After 500 h from inoculation, the power density drops sharply as glucose is depleted in the anodic compartment. The discharge duration is much longer than those of the previously reported *E. coli* MFCs under the same conditions.[38–40] This remarkable improvement indi-

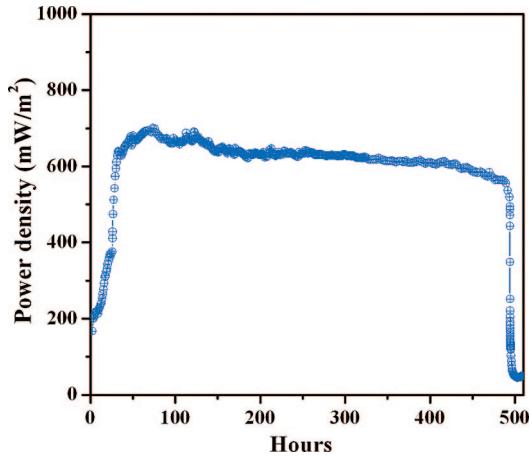

Figure 8. Constant-load discharge curves of MFC with 30 wt % PANI/TiO_2 composite anode.

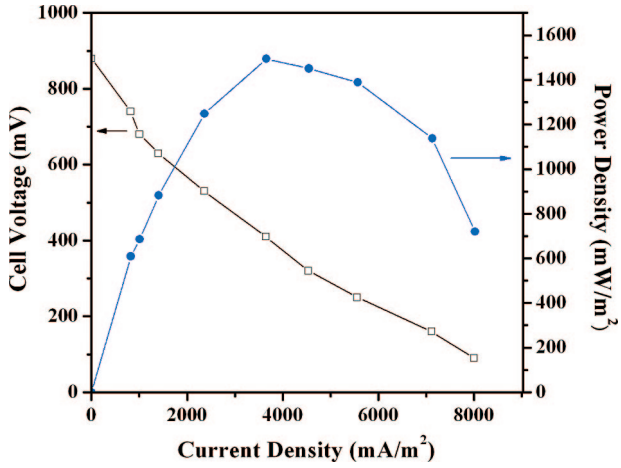

Figure 9. Power output and polarization curve of MFC with 30 wt % PANI/TiO_2 composite anode.

cates high energy conversion efficiency, likely resulting from the *E. coli* biofilm formed on the electrode surface, as discussed above. To determine the power output, various resistances (10–5000 Ω) were used as external loads, and the polarization curve and the power output of the MFC (Figure 9) show that the open-circuit potential is 880 mV and the maximum power output is 1495 mW/m^2, corresponding to a current density of 3650 mA/m^2 at a cell potential of 410 mV. As the maximal power density of *E. coli*-catalyzed MFCs[38] reported to date is 760 mW/m^2, the PANI/TiO_2 nanocomposite anode in our work significantly improves the power density by almost 2-fold. This new composite anode also has greater power density than the CNT/PANI composite we have previously reported.[14] The results demonstrate that the nanoporous PANI/TiO_2 composite with optimal PANI content (30 wt %) can be a superior anode material in a MFC, giving a high power output.

CONCLUSIONS

We present here a unique nanostructured PANI/TiO_2 composite with large specific surface area, uniform nanopore distribution, and good biocatalytic performance. The catalytic performance of the composite anode in microbial fuel cells can be optimized by adjusting the PANI percentage in the composite, and the composite with 30 wt % PANI gives the highest bio- and electrocatalytic performance. In comparison to the reported works, the composite anode delivers 2-fold higher power output (1495 mW/m^2) in an *E. coli* MFC and thus has great potential to be used as an anode for a high-power MFC. This work may also provide a new universal approach for improving other MFCs. The application of this material in mediatorless MFCs is under investigation in the author's laboratory. Although direct electron transfer between the nanocomposite and *E. coli* has been observed, its mechanism is not very clear and is further explored with both electrochemical and biological experimental approaches, which will be presented in another report.

METHODS

Synthesis of PANI/TiO_2 Composite. The mesoporous structured TiO_2 was synthesized by a sol–gel-assisted hydrothermal method as in our previous work.[20] After the TiO_2 was obtained, different volumes of aniline were injected into 50 mL of an aqueous TiO_2 dispersion with 1 M hydrochloric acid under ultrasonic operation to reduce agglomeration. Ammonium peroxydisulfate (APS) solution with a mole ratio of 1:1.25 monomer:APS was added dropwise into the mixture with constant stirring at 0–5 °C. After 12 h of reaction, the precipitate was harvested by filtration and rinsed several times with deionized water and methanol. Finally, the precipitate was vacuum-dried at 60 °C for 24 h, and PANI/TiO_2 composites were obtained.

Characterization of PANI/TiO_2 Composite. The crystal structure of the product was characterized by XRD (Bruker AXS X-ray diffractometer). The morphology was studied with FESEM (JSM-6700, JEOL, Japan) and high-resolution transmission electron microscopy (JEM-2100F, JEOL, Japan). Nitrogen adsorption–desorption experiments were carried out at 77.3 K by using an automated gas sorption system (AUTOSORB-1, Quantachrome Instruments, Boynton Beach, FL). The surface area and pore size distribution were calculated using the Brunauer–Emmett–Teller (BET) equation and Barrett–Joyner–Halenda (BJH) methods, respectively.

Electrode Preparation. The composite powder was mixed with poly(tetrafluoroethylene) solution (1 wt %) to prepare a paste. The paste was then coated on the surface of a nickel foam sheet (1 cm × 1 cm × 0.1 cm) to produce uniform films, followed by pressing with a presser to fabricate the PANI/TiO_2 electrode. The film covered the whole surface of the foam sheet to prevent exposure of nickel to the electrolyte. After drying at 120 °C to remove water, the electrodes were used as the anodes for MFCs.

Bacteria Culture. *E. coli* K-12 (ATCC 29181) was grown anaerobically at 37 °C in a standard glucose medium, which was a mixture contained 10 g of glucose, 5 g of yeast extract, 10 g of $NaHCO_3$, and 8.5 g of NaH_2PO_4 per liter. After growing for 12 h, the bacteria culture in stationary phase was harvested by centrifugation at 4 °C (6000*g*, 5 min). The produced bacteria were washed three times and then suspended in a 0.1 M anaerobic phosphate buffer (pH 7.0) containing 55 mM glucose. The concentration of *E. coli* cells was about 10^9 cells mL^{-1}. Before each test, the suspension was purged over nitrogen for 20 min to remove oxygen from the solution.

Electrochemical Measurements. All electrochemical experiments were carried out with a PGSTAT30 Autolab system (Ecochemie, Utrecht, Netherlands) in a three-electrode cell that consisted of a working electrode, a Ag/AgCl (saturated KCl) reference electrode, and a platinum foil counter electrode. HNQ was chosen as the electron mediator because it can generate higher Coulombic output than commonly used mediators, such as resazurin or thionine.[41] Electrochemical impedance spectra measurements were performed over a frequency range of 0.5 Hz to 100 kHz at −0.2 V, with a perturbation signal of 10 mV.

Acknowledgment. The authors are grateful to the Asian Office of Aerospace Research and Development, U.S. Air Force Office of Scientific Research, for the financial support to this work under contract no. AOARD-05-4073.

REFERENCES AND NOTES

1. Lovley, D. R. Bug juice: Harvesting Electricity with Microorganisms. *Nat. Rev. Microbiol.* **2006**, *4*, 497–508.
2. Holzman, D. C. Microbe Power! *Environ. Health Perspect.* **2005**, *113*, A754–A757.
3. Bullen, R. A.; Arnot, T. C.; Lakeman, J. B.; Walsh, F. C. Biofuel Cells and Their Development. *Biosens. Bioelectron.* **2006**, *21*, 2015–2045.

4. Logan, B. E.; Hamelers, B.; Rozendal, R.; Schrorder, U.; Keller, J.; Freguia, S.; Aelterman, P.; Verstraete, W.; Rabaey, K. Microbial Fuel Cells: Methodology and Technology. *Environ. Sci. Technol.* **2006**, *40*, 5181–5192.
5. Logan, B. E.; Regan, J. M. Electricity-Producing Bacterial Communities in Microbial Fuel Cells. *Trends Microbiol.* **2006**, *14*, 512–518.
6. Park, D. H.; Zeikus, J. G. Improved fuel cell and electrode designs for producing electricity from microbial degradation. *Biotechnol. Bioeng.* **2003**, *81*, 348–355.
7. Lowy, D. A.; Tender, L. M.; Zeikus, J. G.; Park, D. H.; Lovley, D. R. Harvesting Energy from the Marine Sediment-Water Interface II—Kinetic Activity of Anode Materials. *Biosens. Bioelectron.* **2006**, *21*, 2058–2063.
8. Rosenbaum, M.; Zhao, F.; Schroder, U.; Scholz, F. Interfacing Electrocatalysis and Biocatalysis with Tungsten Carbide: A High-Performance, Noble-Metal-Free Microbial Fuel Cell. *Angew. Chem., Int. Ed.* **2006**, *45*, 6658–6661.
9. Rabaey, K.; Verstraete, W. Microbial Fuel Cells: Novel Biotechnology for Energy Generation. *Trends Biotechnol.* **2005**, *23*, 291–298.
10. Syed, A. A.; Dinesan, M. K. Polyaniline—a Novel Polymeric Material—Review. *Talanta* **1991**, *38*, 815–837.
11. Schröder, U.; Nieben, J.; Scholz, F. A Generation of Microbial Fuel Cells with Current Outputs Boosted by More Than One Order of Magnitude. *Angew. Chem., Int. Ed.* **2003**, *115*, 2986–2989.
12. Huguenin, F.; Torresi, R. M.; Buttry, D. A. Lithium Electroinsertion into an Inorganic−Organic Hybrid Material Composed from V_2O_5 and Polyaniline. *J. Electrochem. Soc.* **2002**, *149*, A546–A553.
13. Jang, S. H.; Han, M. G.; Im, S. S. Preparation and Characterization of Conductive Polyaniline/Silica Hybrid Composites Prepared by Sol-gel Process. *Synth. Met.* **2000**, *110*, 17–23.
14. Qiao, Y.; Li, C. M.; Bao, S. J.; Bao, Q. L. Carbon Nanotube/Polyaniline Composite as Anode Material for Microbial Fuel Cells. *J. Power Sources* **2007**, *170*, 79–84.
15. Zhou, H.; Liu, L.; Yin, K.; Liu, S. L.; Li, G. X. Electrochemical Investigation on the Catalytic Ability of Tyrosinase with the Effect of Nano Titanium Dioxide. *Electrochem. Commun.* **2006**, *8*, 1168–1172.
16. Li, X. W.; Wang, G. C.; Li, X. X.; Lu, D. M. Surface Properties of Polyaniline/Nano-TiO_2 Composites. *Appl. Surf. Sci.* **2004**, *229*, 395–401.
17. Vu, Q. T.; Pavlik, M.; Hebestreit, N.; Rammelt, U.; Plieth, W.; Pfleger, J. Nanocomposites Based on Titanium Dioxide and Polythiophene: Structure and Properties. *React. Funct. Polym.* **2005**, *65*, 69–77.
18. Xu, J. C.; Liu, W. M.; Li, H. L. Titanium Dioxide Doped Polyaniline. *Mater. Sci. Eng., C* **2005**, *25*, 444–447.
19. Dey, A.; De, S.; De, A.; De, S. K. Characterization and Dielectric Properties of Polyaniline-TiO_2 Nanocomposites. *Nanotechnology* **2004**, *15*, 1277–1283.
20. Bao, S.-J.; Z., J.-F.; Li, C. M.; Cui, X.-Q.; Qiao, Y.;Guo, J. Novel Nanoporous TiO_2 Electrode for Directly Electrochemistry of glucose oxidase. *Adv. Funct. Mater.* **2007**, in press, http://dx.doi.org/10.1002/adfm.200700728.
21. Bard, A. J.; Faulkner, L. R. *Electrochemical Methods—Fundamentals and Applications*, 2nd ed.; John Wiley & Sons, Inc: New York, 2001; pp 228–242.
22. Song, H. K.; Sung, J. H.; Jung, Y. H.; Lee, K. H.; Dao, L. H.; Kim, M. H.; Kim, H. N. Electrochemical Porosimetry. *J. Electrochem. Soc.* **2004**, *151*, E102–E109.
23. Elliott, J. M.; Owen, J. R. Electrochemical Impedance Characterisation of a Nanostructured (Mesoporous) Platinum Film. *Phys. Chem. Chem. Phys.* **2000**, *2*, 5653–5659.
24. Ghosh, P.; Sarkar, A.; Meikap, A. K.; Chattopadhyay, S. K.; Chatterjee, S. K.; Ghosh, M. Electron Transport Properties of Cobalt Doped Polyaniline. *J. Phys. D* **2006**, *39*, 3047–3052.
25. Li, C. M.; Cha, C. S. Porous carbon composite/enzyme glucose microsensor. *Front. Biosci.* **2004**, *9*, 3324–3330.
26. Zang, J. F.; Li, C. M.; Cui, X. Q.; Wang, J. X.; Sun, X. W.; Dong, H.; Sun, C. Q. Tailoring zinc oxide nanowires for high performance amperometric glucose sensor. *Electroanalysis* **2007**, *19*, 1008–1014.
27. Roller, S. D.; Bennetto, H. P.; Delaney, G. M.; Mason, J. R.; Stirling, J. L.; Thurston, C. F. Electron-Transfer Coupling in Microbial Fuel-Cells. 1. Comparison of Redox-Mediator Reduction Rates and Respiratory Rates of Bacteria. *J. Chem. Technol. Biotechnol. B* **1984**, *34*, 3–12.
28. Lithgow, A. M.; Romero, L.; Sanchez, I. C.; Souto, F. A.; Vega, C. A. Interception of the Electron-Transport Chain in Bacteria with Hydrophilic Redox Mediators. 1. Selective Improvement of the Performance of Biofuel Cells with 2,6-Disulfonated Thionine as Mediator. *J. Chem. Res.-S* **1986**, *5*, 178–179.
29. Austin, L. G. *Fuel Cells: A Review of Government-Sponsered Research 1950–1964*; NASA SP-120; National Aeronautics and Space Administration: Washington, DC, 1967; pp303–320.
30. Pratt, L. A.; Kolter, R. Genetic Analysis of *Escherichia coli* Biofilm Formation: Roles of Flagella, Motility, Chemotaxis and Type I Pili. *Mol. Microbiol.* **1998**, *30*, 285–293.
31. Wall, D.; Kaiser, D. Type IV Pili and Cell Motility. *Mol. Microbiol.* **1999**, *32*, 1–10.
32. Biffinger, J. C.; Pietron, J.; Ray, R.; Little, B.; Ringeisen, B. R. A Biofilm enhanced miniature microbial fuel cell using Shewanella oneidensis DSP10 and oxygen reduction cathodes. *Biosens. Bioelectron.* **2007**, *22*, 1672–1679.
33. Hernandez, M. E.; Newman, D. K. Extracellular electron transfer. *Cell. Mol. Life Sci.* **2001**, *58*, 1562–1571.
34. Reguera, G.; Nevin, K. P.; Nicoll, J. S.; Covalla, S. F.; Woodard, T. L.; Lovley, D. R. Biofilm and nanowire production leads to increased current in Geobacter sulfurreducens fuel cells. *Appl. Environ. Microbiol.* **2006**, *72*, 7345–7348.
35. Reguera, G.; McCarthy, K. D.; Mehta, T.; Nicoll, J. S.; Tuominen, M. T.; Lovley, D. R. Extracellular Electron Transfer via Microbial Nanowires. *Nature* **2005**, *435*, 1098–1101.
36. Gorby, Y. A.; Yanina, S.; McLean, J. S.; Rosso, K. M.; Moyles, D.; Dohnalkova, A.; Beveridge, T. J.; Chang, I. S.; Kim, B. H.; Kim, K. S.; et al. Electrically Conductive Bacterial Nanowires Produced by *Shewanella oneidensis* strain MR-1 and other Microorganisms. *Proc. Natl. Acad. Sci. U.S.A.* **2006**, *103*, 11358–11363.
37. Zhang, T.; Cui, C.; Chen, S.; Ai, X.; Yang, H.; Shen, P.; Peng, Z. A novel mediatorless microbial fuel cell based on biocatalysis of Escherichia coli. *Chem. Commun.* **2006**, *21*, 2257–2259.
38. Zhang, T.; Zeng, Y.; Chen, S.; Ai, X.; Yang, H. Improved Performances of *E. coli*-Catalyzed Microbial Fuel Cells with Composite Graphite/PTFE Anodes. *Electrochem. Commun.* **2007**, *9*, 349–353.
39. Park, D. H.; Zeikus, J. G. Electricity Generation in Microbial Fuel Cells Using Neutral Red as an Electronophore. *Appl. Environ. Microbiol.* **2000**, *66*, 1292–1297.
40. Ieropoulos, I. A.; Greenman, J.; Melhuish, C.; Hart, J. Comparative Study of Three Types of Microbial Fuel Cell. *Enzyme Microb. Technol.* **2005**, *37*, 238–245.
41. Lee, S. A.; Choi, Y.; Jung, S. H.; Kim, S. Effect of Initial Carbon Sources on the Electrochemical Detection of Glucose by *Gluconobacter oxydans*. *Bioelectrochemistry* **2002**, *57*, 173–178.